Finite Larmor radius magnetohydrodynamic analysis of the ballooning modes in tokamaks*

Jiang Hai-Bin(蒋海斌)†, Wang Ai-Ke(王爱科), and Peng Xiao-Dong(彭晓东)

Southwestern Institute of Physics, Chengdu 610041, *China*

(Received 25 February 2010; revised manuscript received 2 April 2010)

In this paper, the effect of finite Larmor radius (FLR) on high n ballooning modes is studied on the basis of FLR magnetohydrodynamic (FLR-MHD) theory. A linear FLR ballooning mode equation is derived in an '$\hat{s}-\alpha$' type equilibrium of circular-flux-surfaces, which is reduced to the ideal ballooning mode equation when the FLR effect is neglected. The present model reproduces some basic features of FLR effects on ballooning mode obtained previously by kinetic ballooning mode theories. That is, the FLR introduces a real frequency into ballooning mode and has a stabilising effect on ballooning modes (e.g., in the case of high magnetic shear $\hat{s} \geq 0.8$). In particular, some new properties of FLR effects on ballooning mode are discovered in the present research. Here it is found that in a high magnetic shear region ($\hat{s} \geq 0.8$) the critical pressure gradient ($\alpha_{\rm c,FLR}$) of ballooning mode is larger than the ideal one ($\alpha_{\rm c,IMHD}$) and becomes larger and larger with the increase of FLR parameter b_0. However, in a low magnetic shear region, the FLR ballooning mode is more unstable than the ideal one, and the $\alpha_{\rm c,FLR}$ is much lower than the $\alpha_{\rm c,IMHD}$. Moreover, the present results indicate that there exist some new weaker instabilities near the second stability boundary (obtained from ideal MHD theory), which means that the second stable region becomes narrow.

Keywords: ballooning mode, finite Larmor radius effect

PACC: 5235P, 5255G

1. Introduction

The ballooning mode is an electromagnetic instability associated with magnetic-field line bending, which is driven by plasma pressure gradient combined with unfavourable magnetic curvature. In the late 1970s, the theory of ideal magnetohydrodynamic (MHD) ballooning modes was well established by the Wentzel–Kramers–Brillouin (WKB) method.[1,2] In the past 30 years a large number of theoretical analyses and numerical simulations on the subject have been carried out. Up to now, the ballooning mode still has been one of the particularly important issues in tokamak plasmas[3−7] because it is one of the possible candidates to impose a limit (obtained from the ideal MHD ballooning mode theory) on the maximum pressure gradient that can be stably confined in tokamaks.[8,9] That is, when β (the ratio of the kinetic pressure to the magnetic pressure) increases to a critical value $\beta_{\rm c}$, unstable ballooning modes are excited in the bad curvature region. Lots of calculation[10−12] have been carried out to determine $\beta_{\rm c}$ from the ideal MHD equations. In these calculations there is a common assumption that the parallel electric field perturbation $E_{\|}$ vanishes.[13] As we know, however, $E_{\|}$ may become finite when kinetic effects, such as finite Larmor radius effect (FLR effect, also referred to as the effect of gyroviscosity[14]), Landau resonances, trapped particles, collisional effects etc, are included. Especially, in the high-n limit these kinetic effects can be significant. It is, therefore, very necessary to examine whether the kinetic effects could significantly modify the stability of the ideal ballooning modes and hence $\beta_{\rm c}$. In the present paper we pay our attention to examining the effects of FLR on the high n ballooning modes.

In 1978 Chu *et al.*[15] used the kinetic energy principle theory to analyse four kinetic effects (FLR, perturbed electron pressure anisotropy, perturbed ion pressure anisotropy and longitudinal electric field) on the ballooning mode. Their analysis comes to the conclusion that the FLR and perturbed electron pressure anisotropy have stabilising effects, whereas the perturbed ion pressure anisotropy and the longitudinal electric field take on the destabilising effects. By minimising the stability effect and maximising the destabilising effect, the $\beta_{\rm c}$ may be 10% lower than that predicted by the MHD theory. Thereafter, Cheng[16] has employed the high n ballooning mode formalism to derive the eigenmode equation for kinetic balloon-

*Project supported by the National Natural Science Foundation of China (Grant Nos. 10775040 and 10775043).

†Corresponding author. E-mail: jianghb@swip.ac.cn

© 2010 Chinese Physical Society and IOP Publishing Ltd

ing modes of arbitrary wavelength in the frequency range $\omega_{\rm ti} < \omega < \omega_{\rm te}$, where $\omega_{\rm ti}$ and $\omega_{\rm te}$ are ion and electron transit frequencies, respectively. The author found that the FLR effects reduce the growth rate but does not stabilise the mode. And besides, the critical $\beta_{\rm c}$ is smaller than the ideal MHD one, except for the case of $\eta_{\rm i} = 0$, where $\eta_{\rm i}$ is the scaled value of ion temperature gradient (ITG). Afterwards, Hirose *et al.*[17,18] made an identification about a kinetic ballooning mode which is driven by a finite ion temperature gradient $\eta_{\rm i}$. They concluded that the $\eta_{\rm i}$ ballooning mode can lower the critical $\alpha_{\rm c}$ significantly at a small magnetic shear.

In general one uses the kinetic theory[19] or gyrokinetic formulation[6,15] to study the kinetic effects on the ballooning mode. However, in as early as the 1960s, attempts were made to use MHD theory instead of kinetic theory to study the system in which FLR effects became important: Roberts and Taylor,[20] and Braginskii[21] independently incorporated the FLR effects into the momentum equation of MHD theory via anisotropic ion (FLR) stress tensor, which is always referred to as finite Larmor radius magnetohydrodynamic (FLR MHD) theory. So far, however, all the subjects that the FLR MHD theory is employed to analyse concentrate on the Rayleigh–Taylor instability in different plasma configurations: Ruden[14] and Huba[22] used this theory to study independently the Rayleigh–Taylor instability in the plasma configuration of two-dimensional geometry. Recently, Qiu *et al.*[23] and Huang *et al.*[24] have used the FLR MHD theory to investigate the Rayleigh–Taylor instability in Z-pinch incompressible plasma with a sheared axial flow and compressible plasma without sheared axial flow. And their results show the FLR effect to be a stabilising factor for Rayleigh–Taylor instability in either incompressible or compressible plasma. In the present paper, we for the first time use FLR MHD theory to analyse the ballooning mode in a more complicated toroidal plasma system. By taking advantage of the simplicity of the FLR-MHD theory model, we derive a linear FLR ballooning mode equation. Because the operator of FLR ballooning mode equation is no longer self-adjoint and hence its eigenvalue is a complex. That is, the present model introduces a real frequency into ballooning mode as shown by the previous kinetic theory.[15] After solving the equation numerically, the results indicate that in a high magnetic shear region ($\hat{s} \geq 0.8$) the FLR has a stabilising effect on ballooning modes. Here it is found that the critical pressure gradient ($\alpha_{\rm c,FLR}$) is larger than the ideal one ($\alpha_{\rm c,IMHD}$) and becomes larger and larger with the increase of FLR parameter b_0. The property may be conducive to the ballooning mode suppression observed on the edge of H mode plasmas,[25] where the shear $\hat{s}$ is high. However, in a low magnetic shear region, when FLR parameter b_0 is small (e.g., $b_0 \leq 0.03$) the FLR ballooning mode is more unstable than the ideal one, and the critical pressure gradient $\alpha_{\rm c,FLR}$ is much lower than the $\alpha_{\rm c,IMHD}$. In particular, the present results indicate that there exist some weaker new instabilities near the second stability boundary, obtained from ideal MHD theory, which means the second stable region becomes narrow.

The remainder of this paper is organised as follows. In Section 2 the fundamental equations are given and linear ballooning mode equation including FLR effects is derived. In Section 3, the numerical results of the eigenmode equation are presented. And a summary is provided in Section 4.

2. Fundamental equations and model

2.1. Fundamental equations

In the present paper, we assume that the plasma is a perfect conducting fluid. So, MHD equations include the convective density evolution equation, the convective pressure evolution equation, and the momentum equation, i.e.,

$$\frac{\partial \rho}{\partial t} + \boldsymbol{V} \cdot \nabla \rho + \rho \nabla \cdot \boldsymbol{V} = 0, \tag{1}$$

$$\frac{\partial p}{\partial t} + \boldsymbol{V} \cdot \nabla p + p \nabla \cdot \boldsymbol{V} = 0, \tag{2}$$

$$\rho \left(\frac{\partial}{\partial t} + \boldsymbol{V} \cdot \nabla \right) \boldsymbol{V} = -\nabla p + \boldsymbol{J} \times \boldsymbol{B} - \nabla \cdot \prod^{f}, \tag{3}$$

where $\prod^{f}$ is the collisionless viscosity tensor due to the FLR effect, which is also known as gyroviscosity. And only the leading order of divergence of the tensor is kept,[26] then we have

$$\begin{aligned} \nabla \cdot \prod^{f} &= \frac{1}{2} \rho \omega_{\rm ci} \rho_{\rm i}^2 \boldsymbol{b} \times \nabla_{\perp}^2 \boldsymbol{V} \\ &= \frac{1}{2} \rho \nu_{\rm g} \boldsymbol{b} \times \nabla_{\perp}^2 \boldsymbol{V}. \end{aligned} \tag{4}$$

This is not real viscosity at all, since the associated viscous stresses are always perpendicular to the velocity, implying that there is no dissipation (i.e., viscous heating) associated with this effect. Here, ρ is the

mass density, $\rho_{\rm i}$ the ion Larmor radius, $\boldsymbol{V}$ the velocity of the plasma, p the pressure and $\omega_{\rm ci} = eB/m_{\rm i}c$ the ion cyclotron frequency, $\boldsymbol{b} = \boldsymbol{B}/B$ is the unit vector in the direction of local magnetic field, and $\nu_{\rm g}$ is defined as the gyroviscosity coefficient: $\nu_{\rm g} = \omega_{\rm ci}\rho_{\rm i}^2$. Furthermore, the magnetic field equations are

$$\frac{\partial \boldsymbol{B}}{\partial t} = \nabla \times (\boldsymbol{V} \times \boldsymbol{B}), \tag{5}$$

$$\nabla \cdot \boldsymbol{B} = 0. \tag{6}$$

Equations (1)–(6) are complete for the ballooning mode analysis in a perfectly conducting plasma by taking the FLR effects into account and hence fundamental equations in the present paper.

2.2. FLR ballooning mode equation

The linearised ballooning mode equation, taking into account the FLR effects, is derived as follows. The plasma variables and the field variables are written as $\boldsymbol{V} = \boldsymbol{V}_0 + \boldsymbol{V}_1$, $p = p_0 + p_1$, and $\boldsymbol{B} = \boldsymbol{B}_0 + \boldsymbol{B}_1$, where the subscripts '0' and '1' denote the equilibrium quantity and the perturbation quantity, respectively. As we know, in static equilibrium, marginally unstable displacements are divergence-free,[27] so that the incompressible condition

$$\nabla \cdot \boldsymbol{V} = 0 \tag{7}$$

can always be used in marginal stability analysis of the ballooning mode.[28] We obtain the usual linearised MHD equations of static plasma from the Eqs. (1)–(7) respectively,

$$\frac{\partial \rho_1}{\partial t} + \boldsymbol{V}_1 \cdot \nabla \rho_0 = 0, \tag{8}$$

$$\frac{\partial p_1}{\partial t} + \boldsymbol{V}_1 \cdot \nabla p_0 = 0, \tag{9}$$

$$\begin{aligned} &\rho_0 \frac{\partial}{\partial t}\boldsymbol{V}_1 \\ &= -\nabla p_1 + (\nabla \times \boldsymbol{B}_1) \times \boldsymbol{B}_0 + (\nabla \times \boldsymbol{B}_0) \times \boldsymbol{B}_1 \\ &\quad - \frac{1}{2}\rho_0 \nu_{\rm g} \boldsymbol{b}_0 \times \nabla_\perp^2 \boldsymbol{V}_1, \end{aligned} \tag{10}$$

$$\frac{\partial \boldsymbol{B}_1}{\partial t} = \nabla \times (\boldsymbol{V}_1 \times \boldsymbol{B}_0), \tag{11}$$

$$\nabla \cdot \boldsymbol{B}_1 = 0, \tag{12}$$

and

$$\nabla \cdot \boldsymbol{V}_1 = 0. \tag{13}$$

To consistently introduce our ordering scheme, we expand all perturbations in powers of $1/n$, where n is the toroidal mode number, according to

$$A_1 = A_1^{(0)} + (1/n)\, A_1^{(1)} + \ldots, \tag{14}$$

where superscripts (0), (1), ... denote the order of the perturbations. For representing ballooning-type instabilities, the covering space concept is invoked so that any perturbation $A_1^{(k)}$ is expressed as[2,29]

$$\begin{aligned} A_1^{(k)} &= \hat{A}_1^{(k)}\left(x_\perp, x_\parallel\right) \exp\left[-{\rm i}\omega t + {\rm i}nS\left(x_\perp\right)\right], \\ &\quad k = 0, 1, 2 \ldots, \end{aligned} \tag{15}$$

where $x_\perp$ and $x_\parallel$ denote the coordinates across and along the magnetic field lines respectively, and S is the eikonal representation accounting for the rapid cross-field variations. Furthermore, for the sake of the existence of non-zero solutions we might as well assume the gyroviscosity coefficient $\nu_{\rm g}$ to be of the order of $o\left(1/n\right)$, i.e.,

$$\nu_{\rm g} = o\left(1/n\right). \tag{16}$$

Equations (8)–(13) are now consistently solved up to order n. According to Eq. (11) the vector ∇S has no component along the unperturbed magnetic field, i.e., $\boldsymbol{B}_0 \cdot \nabla S = 0$.[4,15] The constraint from momentum balance up to order n leads to

$$p_1^{(0)} + \boldsymbol{B}_0 \cdot \boldsymbol{B}_1^{(0)} = \frac{1}{2}\left({\rm i}n\right)\rho \nu_{\rm g} \hat{\boldsymbol{V}}_1^{(0)} \cdot (\boldsymbol{b}_0 \times \nabla S). \tag{17}$$

From the linearised continuity equation (8), energy balance equation (9), momentum balance equation (10), and Maxwell's equations (11) and (12), we obtain the solutions to order n

$$\nabla S \cdot \boldsymbol{V}_1^{(0)} = 0, \tag{18}$$

and

$$\nabla S \cdot \boldsymbol{B}_1^{(0)} = 0. \tag{19}$$

Equation (18) comes from the energy balance equation to order n. However, it is also the $o\left(n\right)$ of the divergence of $\boldsymbol{V}_1$. That is, physically this ordering scheme implies an incompressible motion in leading order. By using the features of Eqs. (18) and (19), it is convenient to express the zeroth-order perturbations as[28]

$$\begin{aligned} \boldsymbol{V}_1^{(0)} &= \hat{\boldsymbol{V}}_1^{(0)} \exp\left(-{\rm i}\omega t + {\rm i}nS\right) \\ &= \left(\hat{V}_\parallel^{(0)} \frac{\boldsymbol{B}_0}{B_0} + \hat{V}_\perp^{(0)} \frac{\boldsymbol{B}_0 \times \nabla S}{|B_0|^2}\right) \\ &\quad \times \exp\left(-{\rm i}\omega t + {\rm i}nS\right), \end{aligned} \tag{20}$$

and

$$\begin{aligned} \boldsymbol{B}_1^{(0)} &= \hat{\boldsymbol{B}}_1^{(0)} \exp\left(-{\rm i}\omega t + {\rm i}nS\right) \\ &= \left(\hat{B}_\parallel^{(0)} \frac{\boldsymbol{B}_0}{B^2} + \hat{B}_\perp^{(0)} \frac{\boldsymbol{B}_0 \times \nabla S}{|\nabla S|^2}\right) \\ &\quad \times \exp\left(-{\rm i}\omega t + {\rm i}nS\right). \end{aligned} \tag{21}$$

In the same way, Eqs. (8)–(13) are solved to order $o(1)$ and yields, respectively,

$$\nabla \cdot \hat{\boldsymbol{V}}_1^{(0)} = -\mathrm{i}\hat{\boldsymbol{V}}_1^{(1)} \cdot \nabla S, \tag{22}$$

$$\hat{p}_1^{(0)}(-\mathrm{i}\omega) = -\hat{\boldsymbol{V}}_1^{(0)} \cdot \nabla p_0, \tag{23}$$

$$\hat{\boldsymbol{B}}_1^{(0)}(-\mathrm{i}\omega) = \boldsymbol{B}_0 \cdot \nabla \hat{\boldsymbol{V}}_0^{(0)} - \left(\hat{\boldsymbol{V}}_0^{(0)} \cdot \nabla\right) \boldsymbol{B}_0, \tag{24}$$

and

$$\begin{aligned} &\rho_0 \hat{\boldsymbol{V}}_1^{(0)}(-\mathrm{i}\omega) \\ &= -\nabla\left(\hat{p}_1^{(0)} + \boldsymbol{B}_0 \cdot \hat{\boldsymbol{B}}_1^{(0)}\right) - \mathrm{i}\left(\hat{p}_1^{(1)} + \boldsymbol{B}_0 \cdot \hat{\boldsymbol{B}}_1^{(1)}\right) \nabla S \\ &+ \left(\boldsymbol{B}_0 \cdot \nabla\right) \hat{\boldsymbol{B}}_1^{(0)} + \left(\hat{\boldsymbol{B}}_1^{(0)} \cdot \nabla\right) \boldsymbol{B}_0 - \frac{1}{2}\mathrm{i}\rho_0 n \nu_\mathrm{g} \boldsymbol{b}_0 \\ &\times \hat{\boldsymbol{V}}_1^{(0)} \nabla_\perp^2(S) + \frac{1}{2}\rho_0 n \nu_\mathrm{g} \boldsymbol{b}_0 \times \hat{\boldsymbol{V}}_1^{(1)} |\nabla S|^2. \end{aligned} \tag{25}$$

Scalarly multipling Eqs. (24) and (25) with $\boldsymbol{B}_0 \times \nabla S$ and using Eqs. (17)–(22), we obtain the following two equations:

$$\hat{B}_\perp^{(0)} = -\frac{1}{\mathrm{i}\omega} \frac{|\nabla S|^2}{\boldsymbol{B}_0^2} \left(\boldsymbol{B}_0 \cdot \nabla\right) \hat{V}_\perp^{(0)} \tag{26}$$

and

$$\begin{aligned} &\rho_0 |\nabla S|^2 \hat{V}_\perp^{(0)}(-\mathrm{i}\omega) \\ &= B_0^2 \left(\boldsymbol{B}_0 \cdot \nabla\right) \hat{B}_\perp^{(0)} - 2\left(\boldsymbol{B}_0 \times \nabla S \cdot \boldsymbol{\kappa}\right) \hat{p}_1^{(0)} \\ &+ \frac{1}{2}\rho_0 \nu_\mathrm{g} (\mathrm{i}n) |\nabla S|^2 \boldsymbol{B}_0 \cdot \nabla \hat{V}_\parallel^{(0)}. \end{aligned} \tag{27}$$

Similarly, scalarly multipling Eq. (25) with $\boldsymbol{B}_0$ we have

$$\rho_0 \hat{V}_\parallel^{(0)}(-\mathrm{i}\omega) = \hat{B}_\perp^{(0)} \frac{|B_0|}{|\nabla S|^2} \nabla \times \boldsymbol{B}_0 \cdot \nabla S. \tag{28}$$

Using Eq. (20), we rewrite Eq. (23) as

$$\hat{p}_1^{(0)} = \frac{1}{\mathrm{i}\omega} \frac{\boldsymbol{B}_0 \times \nabla S \cdot \nabla p_0}{B_0^2} \hat{V}_\perp^{(0)}. \tag{29}$$

Substituting Eqs. (26), (28), and (29) into Eq. (27) we have a linearised ballooning mode equations with variable $\hat{V}_\perp^{(0)}$

$$\begin{aligned} &\boldsymbol{B}_0 \cdot \nabla \left[\frac{|\nabla S|^2}{B_0^2} \left(\boldsymbol{B}_0 \cdot \nabla\right) \hat{V}_\perp^{(0)}\right] \\ &+ \left[D_\mathrm{k} + G_\mathrm{k}\omega + \rho_0 \frac{|\nabla S|^2}{B_0^2}\omega^2\right] \hat{V}_\perp^{(0)} \\ &- \frac{1}{\omega} M_\mathrm{k} \boldsymbol{B}_0 \cdot \nabla \left[\left(\frac{\nabla \times \boldsymbol{B}_0 \cdot \nabla S}{|B_0|} \left(\boldsymbol{B}_0 \cdot \nabla\right) \hat{V}_\perp^{(0)}\right)\right] \\ &= 0, \end{aligned} \tag{30}$$

where

$$D_\mathrm{k} = 2\frac{\boldsymbol{B}_0 \times \nabla S \cdot \boldsymbol{\kappa}}{B_0^2} \frac{\boldsymbol{B}_0 \times \nabla S \cdot \nabla p_0}{B_0^2}, \tag{31}$$

$$G_\mathrm{k} = n\rho \frac{\boldsymbol{B}_0 \times \nabla S \cdot \boldsymbol{\kappa}}{B_0^2} \frac{|\nabla S|^2}{B_0} \nu_\mathrm{g}, \tag{32}$$

and

$$M_\mathrm{k} = \frac{1}{2} n \frac{|\nabla S|^2}{B_0^2} \nu_\mathrm{g}, \tag{33}$$

with $\boldsymbol{\kappa} = \boldsymbol{b}_0 \cdot \nabla \boldsymbol{b}_0$ being the magnetic field line curvature.

2.3. Eikonal representation

In the present work, the perturbations we are interested in are characterised by short perpendicular and long parallel vavelengths, i.e., $k_\perp \rho_\mathrm{i} \sim 1$ and $k_\parallel \rho_\mathrm{i} \sim o(\rho_\mathrm{i}/L)$, where L is the characteristic scale length of the equilibrium variations. Hence, it is suited to adopt the eikonal representation for perturbation A_1:

$$\begin{aligned} &A_1(\psi, \chi, \zeta) \\ &= \hat{A}(\psi, \chi) \exp\left[-\mathrm{i}\omega t + \mathrm{i}nS(\psi, \chi, \zeta)\right] \end{aligned} \tag{34}$$

in an orthogonal magnetic flux coordinate system (ψ, χ, ζ), where ψ denotes the flux surface; χ and ζ refer to the poloidal angle and the toroidal angle; $\hat{A}$ represents the slow variations along the field line. The specific form for S is determined by the requirement for $k_\parallel \rho_\mathrm{i} \sim o(\rho_\mathrm{i}/L)$, which implies

$$\boldsymbol{B}_0 \cdot \nabla S = 0. \tag{35}$$

So, the solution of Eq. (35) in a straight field-line coordinate system can be constructed as the following form:[30]

$$S = \zeta - q(\psi)\chi + k(\psi), \tag{36}$$

where the flux surface quantities $q(\psi)$ and $k(\psi)$ correspond to the safety factor and radial wavenumber, respectively. It should be noted that the radial wavenumber $k(\psi)$, in general is a function to be determined by a higer-order radial non-local analysis,[30,31] but in the present work it appears just as a parameter.

2.4. Shifted-circle model

In order to study the effect of the FLR on the ballooning mode we need to further simplify ballooning equation (30). In this paper the shifted-circle model is used to simplify it. The standard shifted-circle model is obtained by considering a low-beta equilibrium in which the pressure varies rapidly in a thin radial shell.[1,32] Then the global geometry of the equilibrium is approximately unchanged from the low-beta shifted-circle equilibrium of Shafranov.[33] The equilibrium is solved only to the second order in $\varepsilon = a/R$,

where a is the minor radius and R is the major radius of the torus. Therefore, the Grad–Shafranov equation is transformed into two ordinary differential equations. One is an equation about the poloidal magnetic flux $\psi(r)$: solving this equation is essentially equivalent to calculating the magnetic flux of a cylindrical current-carrying plasma column, the other is an equation which is used to determine the Shafranov shift.[34,35] Although this simplified equivalent model is not so exact as the Solov'ev-type solution[36,37] which can describe the axisymmetric toroidal equilibrium with an arbitrary aspect ratio and large elongation and triangularity, this approach reproduces some important features of the ballooning modes, and hence has been proved to be useful in the study of ballooning modes.

The coordinates of the flux surface are then given by

$$R = R_0 + \Delta(r) + r\cos\theta \tag{37}$$

and

$$Z = r\sin\theta, \tag{38}$$

where R_0 is the major radius at the magnetic axis, Z is the vertical axis, $\Delta(r)$ the Shafranov shift function, r the minor radius, and θ the poloidal angle. The local coordinates (r,θ) has the Jacobian

$$J_0 = Rr\left[1 + \Delta'(r)\cos\theta\right]. \tag{39}$$

Here we have used the prime to denote the first order derivative with respect to r. The pressure gradient parameter α is related to $\Delta(r)$ by[1]

$$\alpha = -r\Delta'', \tag{40}$$

where, similarly, Δ'' represents the second order derivative of $\Delta(r)$ with respect to r. After some algebra we obtain the following transformation regulations in the non-orthogonal coordinates (r,θ):

$$|\nabla S|^2 = (q/r)^2\left[1 + (\hat{s}\theta + \alpha\sin\theta - k_{\rm r}r)^2\right], \tag{41}$$

$$(\boldsymbol{B}\times\nabla S)\cdot\boldsymbol{\kappa} = (|\boldsymbol{B}|\,\kappa_n + \nabla S\cdot\nabla\psi\kappa_{\rm g})\frac{B}{|\nabla\psi|}, \tag{42}$$

$$\kappa_n = -\frac{B_\zeta^2}{B^2}\frac{\cos\theta}{R} - \frac{1}{r}\frac{B_\chi^2}{B^2}, \tag{43}$$

$$\kappa_{\rm g} = \frac{B_\zeta}{B}\frac{\sin\theta}{R}, \tag{44}$$

$$\nabla S\cdot\nabla\psi = \frac{{\rm d}S}{{\rm d}r}\left(\frac{{\rm d}\psi}{{\rm d}r}\right)^2. \tag{45}$$

Substituting Eqs. (41)–(45) into Eq. (30), we have the following ballooning eigenmode equation:

$$\frac{\partial}{\partial\theta}\left(f\frac{\partial}{\partial\theta}F\right) + {\rm i}\frac{1}{\Omega}\varepsilon b_{\rm i}\frac{\partial^2}{\partial\theta^2}F + {\rm i}\tau b_{\rm i}\Omega\sigma F + (-\Omega^2 f + h)F = 0, \tag{46}$$

where $\sigma = \cos\theta + \sin\theta\,(\hat{s}\theta - \alpha\sin\theta - k_{\rm r}r)$, $f = 1 + (\hat{s}\theta - \alpha\sin\theta - k_{\rm r}r)^2$, $\tau = -\nu_{\rm g}/\omega_{\rm A}r^2$, $\varepsilon = r\alpha\omega_{\rm ci}/2Rq^3\omega_{\rm A}$, $h = \alpha[\cos\theta + \sin\theta\,(\hat{s}\theta - \alpha\sin\theta - k_{\rm r}r)]$, and $b_{\rm i} = k_\perp^2\rho_{\rm i}^2$. In the above equations, $F = \hat{V}_\perp^{(0)}/R^2B_{0\chi}$ is the eigenfuncton of the ballooning mode, $\Omega = -{\rm i}\omega/\omega_{\rm A}$ is the normalised eigenvalue, q is the safety factor, $\hat{s} = (r/q)\,{\rm d}q/{\rm d}r$ is the surface average magnetic shear, $\alpha = -2Rq^2p'(r)/B_{\rm axis}^2$ is the pressure gradient, $\omega_{\rm A} = V_{\rm A}/qR$ is the Alfven transit frequency over the connection length, $B_{0\chi}$ is the equilibrium poloidal magnetic field, and $B_{\rm axis}$ is the toroidal magnetic field at magnetic axis. The perpendicular wavenumber can be expressed as[15]

$$\begin{aligned} k_\perp^2 &= n^2|\nabla S|^2 \\ &= n^2(q/r)^2\left[1 + (\hat{s}\theta - \alpha\sin\theta - n_{\rm k}K)^2\right], \end{aligned} \tag{47}$$

where $K = k_{\rm r}a$ is the normalised radial wavenumber and $n_{\rm k} = r/a$. By using Eq. (47), we rewrite the term $b_{\rm i}$ in Eq. (46) as

$$\begin{aligned} b_{\rm i} &= k_\perp^2\rho_{\rm i}^2 \\ &= k_\theta^2\rho_{\rm i}^2\left[1 + (\hat{s}\theta - \alpha\sin\theta - n_{\rm k}K)^2\right] \\ &= b_0\left[1 + (\hat{s}\theta - \alpha\sin\theta - n_{\rm k}K)^2\right]. \end{aligned} \tag{48}$$

Here we should point out that $b_0 \equiv k_\theta^2\rho_{\rm i}^2 = \nu_{\rm g}n^2(q/r)^2/\omega_{\rm ci}$ is the FLR parameter which can directly reflect the gyroviscosty effects on the ballooning modes. It should be noted that on the one hand the FLR effect $k_\perp^2\rho_{\rm i}^2$ is not a given parameter but a function of the ballooning angle θ as shown in Fig. 1; on the other hand, it is also a function of normalised radial wavenumber K as shown in Fig. 1(b). That is, when the radial wavelength is very short ($K >> 1$) the FLR effects ($k_\perp^2\rho_{\rm i}^2$) on the left- and the right-hand side at position $\theta = 0$ are unsymmetrical. Furthermore, it can be seen that the FLR effect $k_\perp^2\rho_{\rm i}^2$ is closely related to magnetic shear $\hat{s}$.

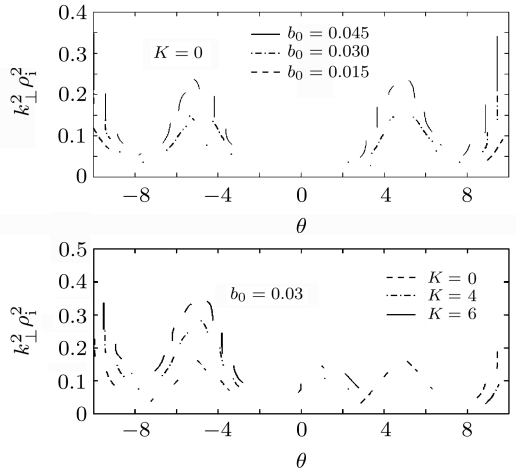


Fig. 1. FLR effects $k_\perp^2\rho_i^2$ in the ballooning modes for different values of FLR parameter b_0 and normalised radial wavenumber K.

Equation (46) is a new result of the present paper. When $b_0 = 0$ (namely, without consideration of the gyroviscosty effect), both the second and the third terms on the left-hand side of Eq. (46) vanish, hence we recover the ideal ballooning equation[1] without FLR effects

$$\frac{\partial}{\partial\theta}\left(f\frac{\partial}{\partial\theta}F\right) + (-\Omega^2 f + h)F = 0. \tag{49}$$

3. Numerical results

Because of the gyroviscosity of the finite Larmor radius effect, the operator of Eq. (46) is no longer self-adjoint when compared with the ideal ballooning equation, and hence its eigenvalue is a complex. That is, the FLR effect introduces a real frequency[22,38] into an unstable ballooning mode. In what follows, we use γ/ω_A to denote the normalised growth rate of the FLR ballooning mode, Ω_r/ω_A the normalised real frequency, F_r the real part of the eigenfunction, and F_i the imaginary parts. In the same way as in most previous work on ballooning modes, we use shooting code analysis to numerically solve Eq. (46) with following boundary conditions:

$$F(\theta = \pm\infty) = 0. \tag{50}$$

First of all, we obtain a group of FLR ballooning eigenfunctions at a usual unstable point ($\hat{s} = 1.0$, $\alpha = 1.0$) with different values of parameter b_0 reflecting the FLR effect as shown in Fig. 2. In order to compare our present mode with the ideal ballooning mode, we first analyse the case of the normalised radical wavenumber parameter $K = 0$.

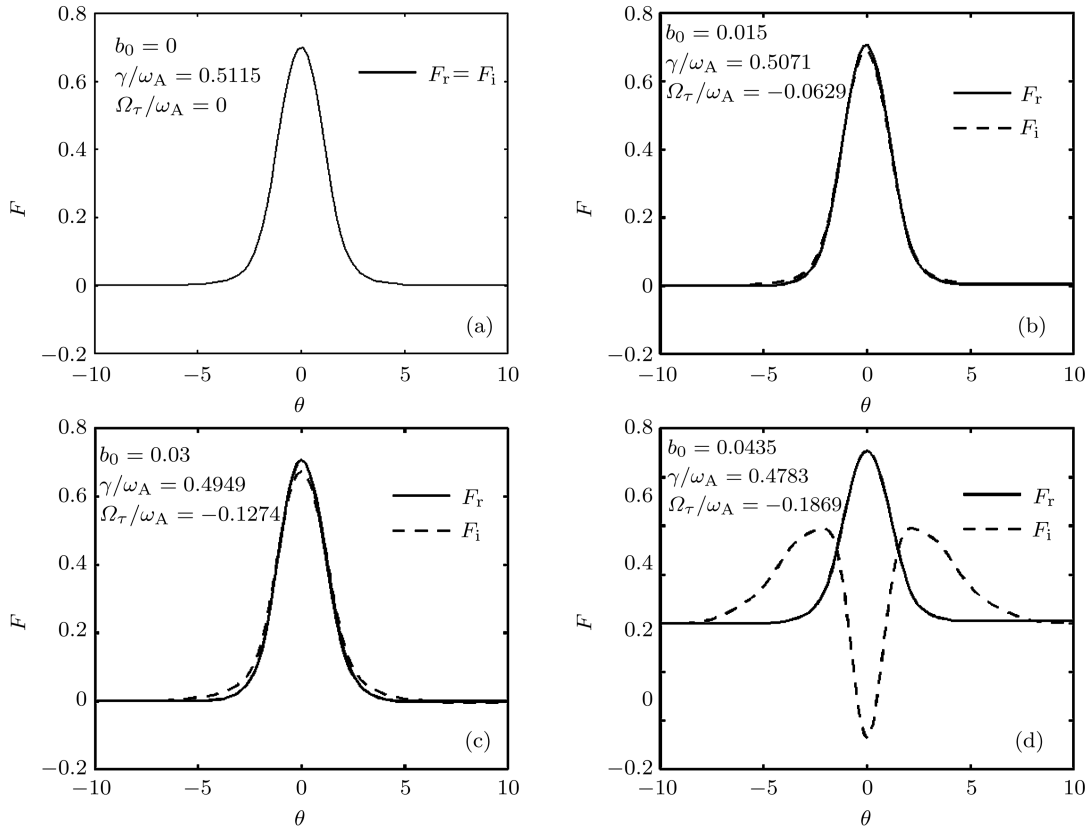


Fig. 2. Eigenfunctions of ballooning modes for different values of FLR parameter b_0. The solid (dash) lines represent the real (imaginary) parts.

Figure 2 can represent the FLR effect on the ballooning mode in many aspects. Figure 2(a) corresponds to the case of $b_0 = 0$, namely, the eigenfunction and eigenvalue of the ideal ballooning mode. It clearly shows that the ideal ballooning instability has a zero real frequency (normalised real frequency $\Omega_{\rm r}/\omega_{\rm A} = 0$) and normalised growth rate $\gamma/\omega_{\rm A} = 0.5115$. In Figs. 2(b)–2(d), by making the parameter b_0 increase from $b_0 = 0.015$ to $b_0 = 0.0435$ we find that the FLR effect does not change the symmetry structure of the eigenfunction (both the real part $F_{\rm r}$ and imaginary part $F_{\rm i}$) on the left- and right-hand side at position $\theta = 0$, except the real part $F_{\rm r}$ (the solid lines in Fig. 2) of eigenfunction separating from the imaginary part $F_{\rm i}$ (the dash lines in Fig. 2). As mentioned above, the FLR effect will introduce a real frequency into the ballooning mode. That is, there exist nonzero real frequencies [$\Omega_{\rm r}/\omega_{\rm A} = -0.0629, \ -0.1274, \ -0.1869$ in Figs. 2(b)–2(d), respectively]. In particular, with the increase of the value of the FLR parameter b_0, the growth rate is smaller and smaller and the separation of the real part from the imaginary part of eigenfunction is more and more prominent. These features of the FLR are again demonstrated in Figs. 3 and 4 in which the normalised growth rate $\gamma/\omega_{\rm A}$ and normalised real frequency $\Omega_{\rm r}/\omega_{\rm A}$ are plotted versus FLR parameter b_0 for different radial wavelengths.

In the present paper, we analyse the FLR effects on the eigenvalue of the ballooning modes in two special regions: the high shear region $\hat{s} = 1.4$ and the low shear region $\hat{s} = 0.25$. From Fig. 3, it can be seen that the curves of the normalised growth rate $\gamma/\omega_{\rm A}$ monotonically decrease, indicating that the FLR effect can suppress the growth rate of the ballooning mode. However, with the increase of the FLR parameter b_0, the depressed effects becomes weaker and weaker, which is in accordance with the results in Fig. 2 and qualitatively consistent with Cheng's conclusion[16] that the FLR effects reduce the growth rate but do not stabilise the mode. Furthermore, when we enhance the value of FLR parameter b_0, a reversal (from negative to positive) of the real frequency first appears, and finally tends to a stable frequency. However, there are some differences of the FLR effects on the ballooning mode when the shear is low ($\hat{s} = 0.2$). From Fig. 4, we can see that in a low magnetic shear region the FLR effect enhances the growth rate of the unstable mode slightly when FLR parameter b_0 is small (e.g., $b_0 < 0.03$).

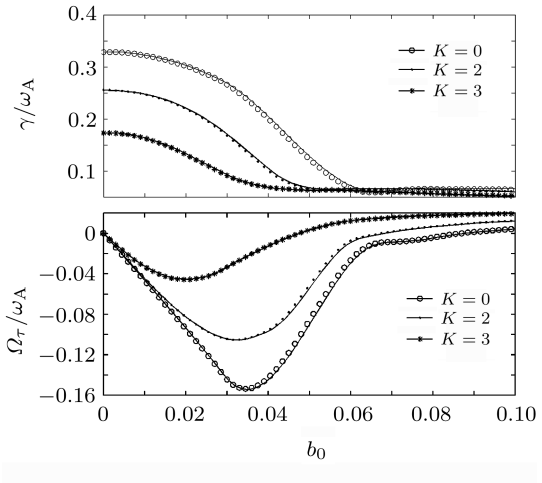


Fig. 3. Dependences of the growth rate (a) and frequency (b) on the FLR parameter b_0 for different values of normalised radial wavenumber K when $\hat{s} = 1.4$ and $\alpha = 1.0$.

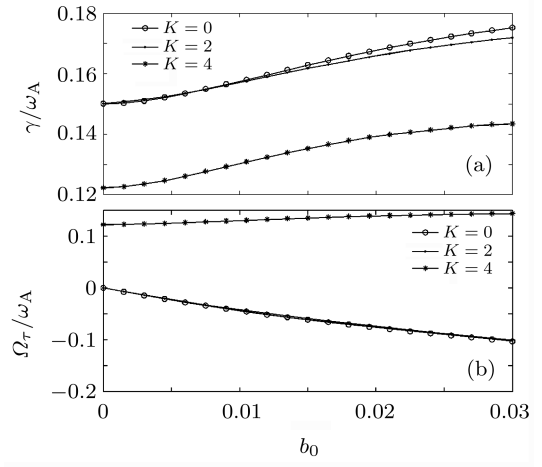


Fig. 4. Dependences of growth rate (a) and frequency (b) on FLR parameter b_0 for different values of normalised radial wavenumber K when $\hat{s} = 0.25$ and $\alpha = 1.0$.

The previous studies[1,2,5] on the ballooning mode have considered merely the case of $k(\psi) = 0$ in Eq. (36) (i.e., the normalised radial wavenumber parameter $K = 0$). From Figs. 3(a) and 4(a), it follows that the ballooning modes with long radial wavelength ($K = 0$) are more unstable than the short ones. Therefore, we need to analyse only the ballooning mode with $K = 0$ in general. However, the characteristic of the eigenfunction cannot be seen in Figs. 3(a) and 4(a).

For this reason, we depict a group of FLR ballooning eigenfunctions (with FLR parameter $b_0 = 0.03$) at the same point ($\hat{s} = 1.0$, $\alpha = 1.0$) for different values of normalised radial normalised wavenumber K as shown in Fig. 5. Obviously, the eigenfunction of the ballooning mode with the normalised radial wavenumber $K = 0$ (Fig. 5(a)) is symmetrical on the

left- and right-hand side at position $\theta = 0$. However, from Figs. 5(b)–5(d), we can see that with the increase of K there appear the drift and the unsymmetry of the corresponding eigenfunction. In Fig. 6 shows the curves for normalised growth rate and normalised real frequency versus normalised radial wavenumber K, where parameters $\hat{s}$ and α are chosen to be $\hat{s} = 1.0$ and $\alpha = 1.0$. From Fig. 6, it can be seen that the growth rate becomes smaller with the increase of K. Therefore, in the following we will analyse the ballooning mode in the case of only $K = 0$.

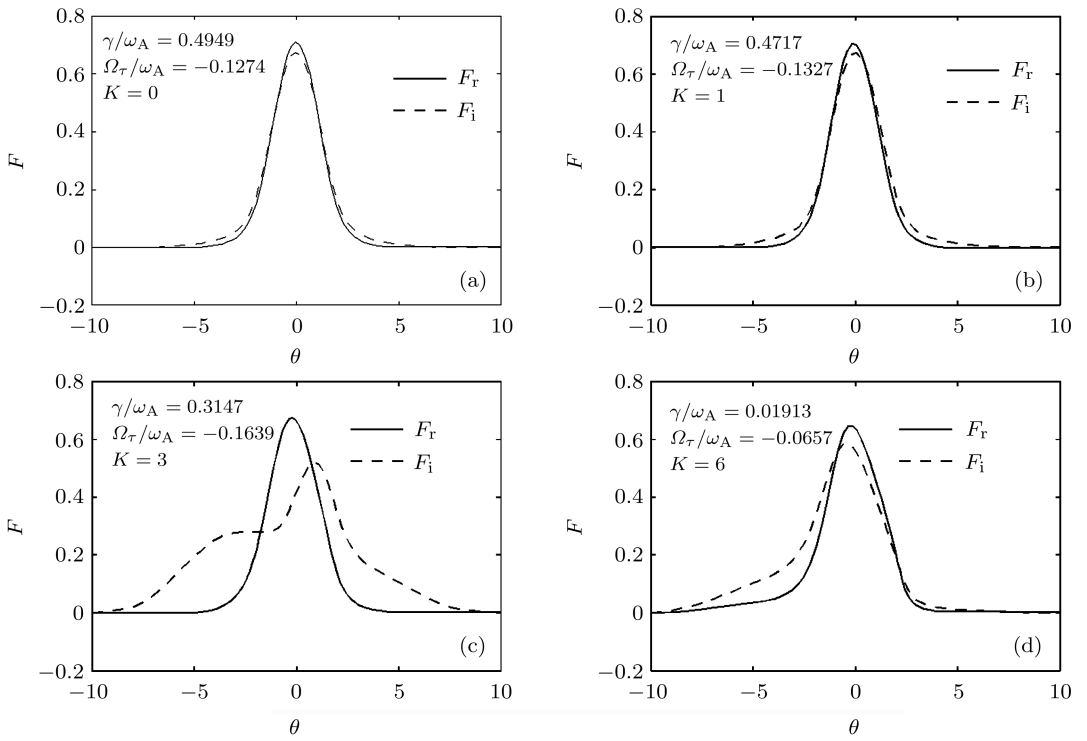


Fig. 5. Eigenfunctions of ballooning modes for different values of normalised wavenumber K when FLR parameter $b_0 = 0.03$. The solid (dash) lines represent the real (imaginary) parts.

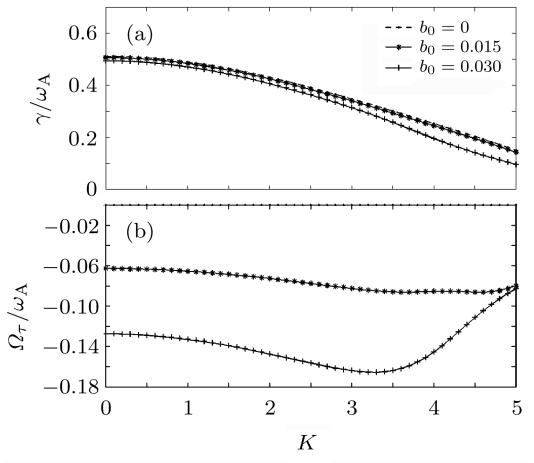


Fig. 6. Dependences of the growth rate (a) and frequency (b) on normalised radial wavenumber K for different values of FLR parameter b_0 when $\hat{s} = 1.0$ and $\alpha = 1.0$.

As described in Ref. [19], there is instability in the MHD second stability regime, driven by a finite ion temperature gradient through the ion resonance at the magnetic drift frequency. It means that the ion resonance effects would reduce the stability regime. Based on the same consideration, we verify that the FLR effects may affect the MHD stability regime. For this purpose we plot the eigenvalues (growth rate and mode frequency normalised by the Alfven frequency ω_A) versus pressure gradient α for high shear $\hat{s} = 1.4$ and low shear $\hat{s} = 0.2$, separately. For comparison, the results obtained from the ideal ballooning mode Eq. (49) are also shown.

From Fig. 7 (for the case of low shear $\hat{s} = 1.4$), it can be seen that the FLR ballooning mode is more stable than the ideal one, which reflects the conventional stabilising effect of the FLR. But, in the low shear region ($\hat{s} = 0.2$) shown in Fig. 8, we can see that the

FLR effect on instability is exactly contrary to that in high shear one. That is, when the FLR parameter b_0 is small (e.g., $b_0 \leq 0.03$) the FLR ballooning mode is more unstable than the ideal one, which can also be found in the analysis of the kinetic theory.[19]

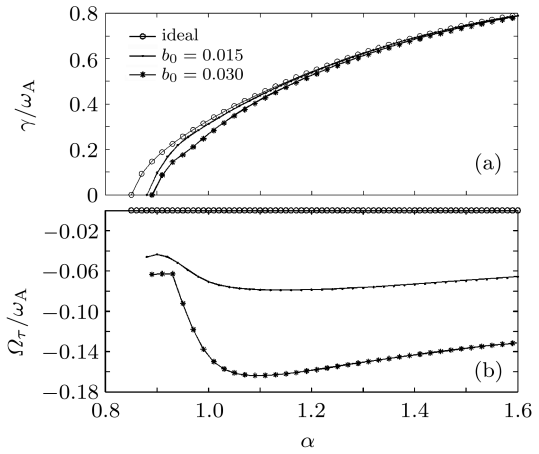


Fig. 7. Curves for growth rate (a) and frequency (b) of the FLR ballooning mode at higher shear, $\hat{s} = 1.4$, for $b_0 = 0.015$ and $b_0 = 0.030$ (denoted by point and asterisk). For comparison, the eigenvalues of the ideal ballooning mode are plotted in this figure (denoted by circle).

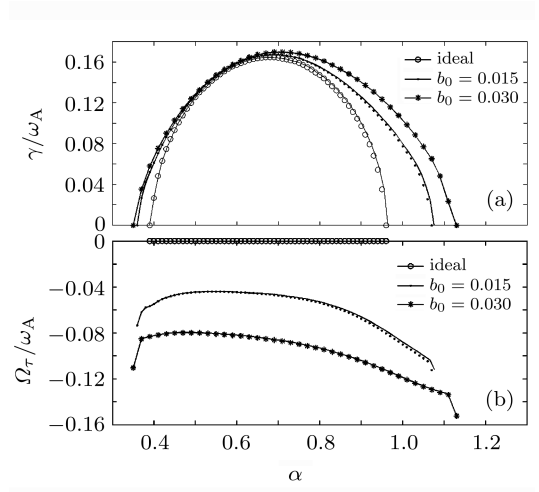


Fig. 8. Curves for growth rate (a) and frequency (b) of the FLR ballooning mode at lower shear, $\hat{s} = 0.2$, for $b_0 = 0.015$ and $b_0 = 0.030$ (denoted by point and asterisk). For comparison, the eigenvalues of the ideal ballooning mode are plotted in this figure (denoted by circle).

In order to obtain a comprehensive understanding, we plot the stability boundary of the FLR ballooning mode in Fig. 9 for different values of FLR parameter b_0. For the comparison with the stability boundary of the ideal ballooning mode, in the FLR MHD theory we focus on the analysis of the most unstable mode with the normalised radial wavenumber $K = 0$. As is well known, the stability of the ideal MHD ballooning mode is fully determined by the two parameters, $\hat{s}$ and α. However, in the FLR MHD theory, the FLR parameter $b_0 = (k_\theta \rho_i)^2$ is introduced as a parameter that modifies the ideal MHD stability diagram. As shown in Fig. 9, in the high shear region the FLR ballooning mode (dashed line and dotted line) has a higher critical value pressure gradient (α_c) than the ideal ballooning mode (solid line), which is the result of the stabilising effect from the FLR. In other words, when the shear is high, we do not find the unstable FLR ballooning mode in the region close to the ideal first stability boundary (see the shadow region in Fig. 9). It reproduces the conclusion obtained in Ref. [39] that the weakly unstable systems can always be stabilised by the FLR effects. However, in the lower magnetic shear region ($\hat{s} \leq 0.8$), the critical α_c of the FLR ballooning mode $\alpha_{c,FLR}$ is significantly lower than $\alpha_{c,IMHD}$, which is similar to the effect induced by the ion magnetic drift resonance.[6] Besides, from Figs. 8 and 9 we can see that there appear some weaker new instabilities near the second stability boundary (obtained from ideal MHD theory), which means the second stable region becomes narrow. However, it should be noted that the ballooning mode still has a second stable region, although the FLR effects reduce it.

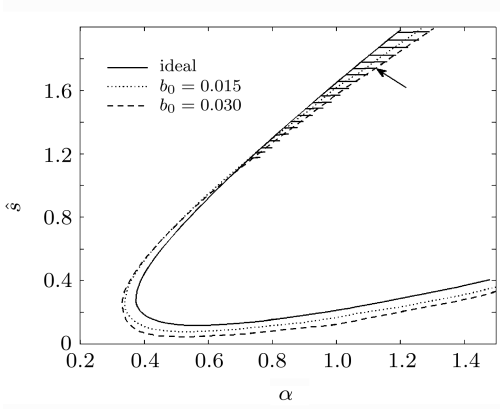


Fig. 9. Stability boundaries of FLR ballooning mode for different values of FLR parameter b_0 (dash line and dot line) and ideal ballooning mode predicted by the ideal MHD theory (solid line).

4. Conclusions

In the present paper, we use the finite Larmor radius magnetohydrodynamic (FLR MHD) theory in the approximation of incompressible fluid to study the high n ballooning modes. Because the FLR (gyroviscosity) effect is included in the present model, the operator of the FLR ballooning mode equation is no

longer self-adjoint when compared with the ideal ballooning mode equation. Thus, the present model introduces a real frequency into the ballooning mode, as done in kinetic theories. In addition, this property is verified by the numerical results in which the eigenvalue has a non-zero real part. In analysing the features of the FLR ballooning mode, it is found that the FLR can hardly affect the eigenmode structure, except the real part $F_{\rm r}$ of eigenfunction separating from the imaginary part $F_{\rm i}$. In a high shear region ($\hat{s} \geq 0.8$) the FLR has a stable effect on ballooning modes, as shown by kinetics theories. Here it is found that the critical pressure gradient $\alpha_{\rm c,FLR}$ is larger than ideal one $\alpha_{\rm c,IMHD}$ and becomes larger and larger with the increase of FLR parameter b_0. The property may be conducive to the ballooning mode suppression, observed in the edge of H-mode plasmas[27] where the shear $\hat{s}$ is high. However, in a low shear region, when the FLR parameter b_0 is small (i.e., $b_0 \leq 0.03$) the FLR ballooning mode is more unstable than the ideal one and accordingly the $\alpha_{\rm c,FLR}$ is much lower than $\alpha_{\rm c,IMHD}$. This phenomenon is similar to one induced by the kinetic effects of the perturbed ion pressure anisotropy, the longitudinal electric field,[16] and the ion magnetic drift resonance.[19] Particularly, the present results indicate that there appear some weaker new instabilities near the second stability boundary (obtained from the ideal MHD theory) when the FLR effect is included. It means the second stable region becomes narrow.

In summary, we for the first time use the FLR MHD theory to study the finite Larmor radium effect on ballooning modes. It reproduces some basic characteristics of ballooning mode, which have been obtained previously by kinetic theories. In addition, some new properties of ballooning mode are discovered when the FLR effect is included.

Acknowledgment

The authors would like to thank Professor Qiu Xiao-Ming for valuable suggestions and helpful discussions.

References

[1] Connor J W, Hastie R J and Taylor J B 1978 *Phys. Rev. Lett.* **40** 396

[2] Dewar R L and Glasser A H 1983 *Phys. Fluid.* **26** 3038

[3] Wilson H R 2004 *Phys. Rev. Lett.* **92** 175006

[4] Connor J W and Hastie R J 2004 *Phys. Rev. Lett.* **92** 075001

[5] Hirose A and Elia M 2003 *Phys. Plasmas* **10** 1195

[6] Joiner N and Hirose A 2008 *Phys. Plasmas* **15** 082107

[7] Kirk A, Koch B, Scannell R, Wilson H R, Counsell G, Dowling J, Herrmann A, Martin R and Walsh M 2006 *Phys. Rev. Lett.* **96** 185001

[8] Dobrott D, Nelson D B, Greene J M, Glasser A H, Chance M S and Frieman E A 1977 *Phys. Rev. Lett.* **39** 943

[9] Coppi B 1977 *Phys. Rev. Lett.* **39** 938

[10] Zohm H, Suttrop W, Blank H J de, Buttery R J, Gates D A, Heikkinen J A, Herrmann W, Kallenbach A, Kass T, Kaufmann M, Kurki-Sonio T, Kurzan B, Maraschek M, Reimerdes H, Ryter F, Salzmann H, Schweinzer J, Stober J, ASDEX-Upgrade, ECRH, ICRH and NBI teams 1997 *Proceedings of the Sixteenth International Conference on Fusion Energy* Montreal 7-11 October 1996 (International Atomic Energy Agency, Vienna) 1997 Vol. 1, p. 439

[11] Janeschitz G, Hubbard A, Igitkhanov Yu, Lingertat J, Osborne T, Pacher H D, Pogutse O P, Post D E, Shimada M, Sugihara M and Suttrop W 1997 *Proceedings of the Twenty Fourth European Physical Society Conference on Controlled Fusion and Plasma Physics* Berchtesgaden 9-13 June 1997 (European Physical Society, Petit-Lancy) 1997 Part III p993

[12] Osborne T H, Groebner R J, Lau L L, Leonard A W, Maingi R, Miller R L, Porter G D, Thomas D M and Waltz R E 1997 *Proceedings of the Twenty Fourth European Physical Society Conference on Controlled Fusion and Plasma Physics* Berchtesgaden 9-13 June 1997 (European Physical Society, Petit-Lancy) 1997 Part III p1101

[13] Dewar R L, Manickam J, Grimm R C and Chance M S 1981 *Nucl. Fusion* **21** 493

[14] Ruden E L 2004 *Phys. Plasmas* **11** 713

[15] Chu M S, Chu C, Guest G, Hsu J Y and Ohkawa T 1978 *Phys. Rev. Lett.* **41** 247

[16] Cheng C Z 1982 *Phys. Fluids* **25** 1020

[17] Hirose A, Zhang L and Elia M 1994 *Phys. Rev. Lett.* **72** 3993

[18] Hirose A, Zhang L and Elia M 1995 *Phys. Plasmas* **2** 859

[19] Tang W M, Connor J W and Hastie R J 1980 *Nuclear Fusion* **20** 1439

[20] Roberts K V and Taylor J B 1962 *Phys. Rev. Lett.* **8** 197

[21] Braginskii S I 1965 *Reviews of Plasma Physics* (New York: Consultants Bureau) Vol. **1** p205

[22] Huba J D 1996 *Phys. Plasmas* **3** 2523

[23] Qiu X M, Huang L and Jian G D 2007 *Phys. Plasmas* **14** 032111

[24] Huang L, Jian G D, Qiu X M, Peng X D and Wang S Q 2008 *Phys. Plasmas* **15** 022103

[25] Wagner F 2007 *Plasma Phys. Controlled Fusion* **49** B1

[26] Kim C B 1993 *Phys. Fluids* B **5** 1516

[27] Waelbroeck F L and Chen L 1991 *Phys. Fluids* B **3** 601
[28] Coper W A 1988 *Plasma Phys. Controlled Fusion* **30** 1805
[29] Grassie K and Krech M 1990 *Phys. Fluids* B **2** 536
[30] Connor J W, Hastie R J and Taylor J B 1979 *Proc. R. Soc.* (London) Ser. A **365** 1
[31] Frieman E A, Rewoldt G, Tang W M and Glasser A H 1980 *Phys. Fluids* **23** 1750
[32] Greene J M and Chance M 1981 *Nuclear Fusion* **21** 453
[33] White R B 1989 *Theory of Tokamka Plasma* (Amsterdam: North-Holland) p132
[34] Shi B R, Lin J L and Li J Q 2007 *Chin. Phys.* **16** 1399
[35] Shi B R and Qu W X 2006 *Chin. Phys.* **15** 1532
[36] Solov'ev L S 1968 *Sov. Phys. JETP* **26** 400
[37] Shi B R 2004 *Plasma Phys. Controlled Fusion* **46** 1105
[38] Rosenbluth M N, Tsai S T, van Dam J W and Engquist M G 1983 *Phys. Rev. Lett.* **51** 1967
[39] Rosenbluth M N, Krall N A and Rostoker N 1962 *Nuclear Fusion Suppl.* Pt. **1** 143